Enhanced mechano-responsive fluorescence in polydiacetylene thin films through functionalization with tetrazine dyes: photopolymerization, energy transfer and AFM coupled to fluorescence microscopy studies

Luca Polacchi, Arnaud Brosseau, Régis Guillot, Rémi Métivier, Clémence Allain

ARTICLE

Enhanced mechano-responsive fluorescence in polydiacetylene thin films through functionalization with tetrazine dyes: photopolymerization, energy transfer and AFM coupled to fluorescence microscopy studies

Received 00th January 20xx,
Accepted 00th January 20xx

DOI: 10.1039/x0xx00000x

Luca Polacchi[a], Arnaud Brosseau[a], Régis Guillot[b], Rémi Métivier[a], Clémence Allain*[a]*

The development of mechano-responsive fluorescent materials is essential for the design and construction of reliable and versatile sensors for mechanical stress. Herein, novel energy transfer-based systems with tetrazine fluorophore and a polydiacetylene (PDA) backbone are synthesized and studied comparatively to a simple polydiacetylene in the form of thin films. Their photopolymerization properties, energy transfer efficiencies and fluorescent response to nanoscale mechanical stimulation are assessed. It is pointed out that the self-assembling group on the PDA chain influences the geometrical arrangement of the chains and the film morphology and, as a consequence, the efficiency and kinetics of polymerization and the energy transfer efficiency. Moreover, we show that the strategy of introducing tetrazine fluorophore provides a new effective route of improving force detectability by fluorescence using polydiacetylenes as mechano-responsive units.

1. Introduction

Mechano-responsive luminescent materials are smart-materials that change their emission properties in the solid state (wavelength, intensity or lifetime) upon appropriate mechanical stimulation, like pressure, rubbing or grinding. This change is ascribable to a modification of the supramolecular packing and intermolecular interactions which affects the electronic energy levels of the fluorophore, or the nature of the emissive species in the material, ultimately resulting in a modified radiative relaxation. [1,2] Several classes of mechano-responsive compounds have already been identified: single organic molecules, [3–5] organometallic complexes [6,7], or polymer composites. [8,9] These materials have attracted considerable attention in the past few years to serve as fluorescent switches, mechanosensors or mechanohistory trackers, but the forces triggering the transition have not been quantified yet, which is a serious limitation for their actual application.

Among the wide variety of smart-materials, polydiacetylenes (PDAs) particularly stand out because of their chromogenic and fluorogenic properties and their outstanding versatility for various applications. They can be obtained by topotactical polymerization via γ-rays, heat or UV radiation at 254 nm, through a 1,4-addition mechanism of properly distanced diacetylene units directly in the solid state, in the form of vesicles in solution or even embedded in polymer matrices.[10] Polymerization is responsible for the first chromogenic transition of these materials because of the formation of long-extended π-conjugated chains, which usually present a characteristic absorption between 600 and 640 nm, responsible for their purple-blue color. It is well known that the so-called blue form undergoes a second drastic color change to a so-called red form, whose absorption band is located between 540 and 580 nm and is weakly fluorescent.[11] The electronic transition is known to be connected with the supramolecular arrangement of the polymer [12] and is triggered by various stimuli like bio- or chemo- specific binding, [13] temperature, pH, ions, solvent detection [14–16] and mechanical forces. [17–22] However, the sensitivity of these systems is dramatically limited by the low fluorescence quantum yields of the stimulated PDA red-form, that can be overcome by adding an appropriate fluorophore to allow energy transfer. Lipophilic BODIPY (boron-dipyrromethene) has been successfully incorporated in PDA liposomes and used as donor to thermally-induced red chains acceptors, whose fluorescence signal is thus amplified.[23] Similarly, an efficient FRET (Förster Resonance Energy Transfer) mechanism is achieved with red-PDA chains, arranged as liposomes in solution, with dansyl fluorophore covalently attached to the DA unit.[24] Alternatively, 1,2,4,5-tetrazine can be used as donor uniquely to blue chains acceptors, resulting in a fluorescence recovery when the polymer is heated and converted to the red form, reducing drastically the spectral overlap between

[a] Université Paris-Saclay, ENS Paris-Saclay, CNRS, PPSM, 91190 Gif-sur-Yvette, France
[b] Université Paris-Saclay, CNRS, Institut de Chimie Moléculaire et des Matériaux d'Orsay, 91405, Orsay, France

Electronic Supplementary Information (ESI) available: synthetic protocols, ^{1}H NMR, ^{13}C NMR, HRMS analyses; crystallographic data, statistical analysis of crystal length and width, thin film thickness estimation from OD, steady state spectroscopy of **DA1**, fluorescence lifetime and additional force-fluorescence tests on **DA1** and **TzDA2**.. See DOI: 10.1039/x0xx00000x

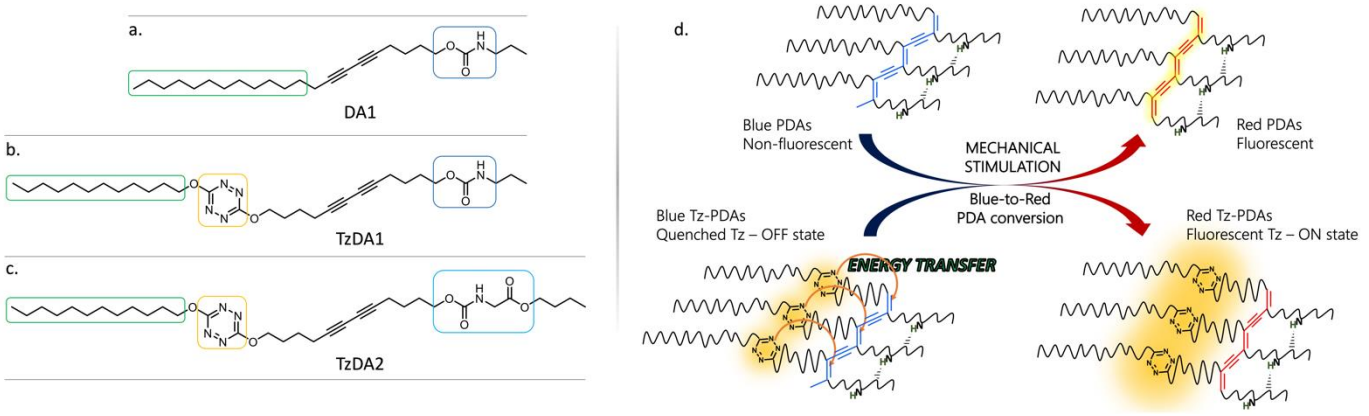

Figure 1. Structure of **DA1** (**a**); **TzDA1** (**b**) and **TzDA2** (**c**). The self-assembling group is highlighted in blue, the tetrazine fluorophore in yellow and the alkyl chain in green. Mechanical force sensing mechanism of simple chain DAs and TzDAs (**d**)

polymer absorption and fluorophore emission.[25, 26] We extended the study of tetrazine-substituted PDAs in regard to their response to mechanical stimulation at the macro- and nano-scale, and showed that the fluorescence recovery was correlated to the friction force applied by atomic force microscopy on thin films.[26] In this study, we widened the investigation to PDA-based materials, showing that the presence of the tetrazine dye in the structure results in a better OFF-to-ON fluorescence contrast for mechanical forces detection at the nanoscale and in a better-suited thin film morphology for this kind of experiment. Moreover, we demonstrate that the self-assembling group of the DA derivative is crucial to tune the film morphology and the spectroscopic properties, especially fluorophore quenching efficiency.

2. Results and discussion

2.1 Molecular design, synthesis and X-ray crystal structure

In this work, two types of polydiacetylene-based mechano-responsive systems have been prepared. **DA1** (Figure 1a) is a simple chain diacetylene with a C12 chain on one side of the acetylene unit, and a urethane moiety on the other. This stands as an analogue of the second type of system, **TzDA1** (Figure 1b), in which a fluorophore is covalently attached. As previously reported in [25], tetrazine was found to be a suitable fluorophore to covalently attach to a diacetylene moiety because of its small size and appropriate fluorescence band (λ_{em} = 560 nm) that overlaps with the absorbance of the blue form of the PDA. The appropriate distance between the monomers for the topotactical polymerization to occur is not exceeded and is ensured by the presence of the same self-assembling groups as **DA1**, a urethane moiety that allows the formation of inter-chain H-bonds, and the alkyl chain. In **TzDA2** (Figure 1c) the terminal group has been modified adding a butyl-ester, similar to the one encountered in the widely studied 3- and 4-BCMU polydiacetylenes.[27–30] The C4 aliphatic chain between the tetrazine dye and the diacetylene in **TzDA1** and **TzDA2** allows combining the mechanoresponsiveness of the PDA chains with an efficient energy transfer from the tetrazine to the blue form of the PDA, by fixing a suitable distance between donor and acceptor while keeping flexibility in the molecular structure. Playing with the chemical structures of these diacetylene derivatives is expected to influence the sample morphology thus to potentially tune their mechanical and photophysical properties, that affect the response to mechanical stimulation at the nanoscale. Simple diacetylenes usually polymerize in a blue non-fluorescent form (λ_{abs} ~ 630 nm). When an external stimulus is applied, the blue form is converted to a red form (λ_{abs} ~ 540 nm), which is weakly fluorescent (λ_{em} = 640 nm, plus a vibronic peak at λ = 560 nm). [31] They constitute thus OFF-to-ON sensors. Tetrazine-substituted diacetylene are instead ON-to-OFF-to-ON systems. In fact, because the fluorescence emission band of tetrazine overlaps with the blue-PDA absorbance, an energy transfer is expected to occur exclusively with the blue form of the PDA. Therefore, the tetrazine fluorescence could switch from the ON state of the monomer to the OFF state of the blue polymer, and back to the ON state when the blue form is converted to the red form and the spectral overlap is lost or strongly decreased (Figure 1d).

2.2 Synthesis of DA1, diacetylene simple chain

DA1 is obtained through a 3 steps synthesis (see SI for detailed protocols). Hex-5-yn-1-yl propyl carbamate is obtained in 82% yield by the reaction of 6-hexynol with propyl isocyanate in refluxed toluene with triethylamine. 1-bromopentadec-1-yne is obtained in 95% yield by bromination of commercially available pentadec-1-yne by N-bromosuccinimide in presence of silver nitrate $AgNO_3$. The terminal alkyne and the bromoalkyne are then coupled unsymmetrically by a Cu(I)-catalyzed Cadiot-Chodkiewicz coupling reaction to give DA1 with 74% yield.[32] Ethylamine is used to both neutralize the resulting bromic acid from the condensation, and as a ligand for the Cu(I) metallic center. A mixture of methanol and water is used to ensure a good solubility of both the acetylenes (organic phase) and the cuprous derivative (aqueous phase).

2.3 Synthesis of TzDA1 and TzDA2, tetrazine-substituted diacetylenes

Commercially available hexyn-1-ol reacts with commercially available isocyanates (1-isocyanatopropane for **TzDA1** and butyl-2-isocyanoacetate for **TzDA2**) with good yields, respectively 82% and quantitative. The resulting terminal alkynes are coupled with 6-bromo-hexyn-1-ol by the copper catalyzed Cadiot-Chodkiewicz reaction in a mixture of DCM/H_2O with butylamine. The resulting diacetylene is then let react at controlled low temperature (5-7°C) in inert atmosphere with the 3-chloro-6-dodecyloxytetrazine. The final product is obtained in acceptable yields, 39% for **TzDA1** and 24% for **TzDA2** (see SI for detailed protocols).

2.4 TzDA1 crystal structure

The X-ray crystal structure of **TzDA1** was obtained on isolated crystals grown by liquid-liquid diffusion method. **TzDA1** monomer is dissolved in acetonitrile (0.5 mM) and the solution is layered on an equivalent volume of distilled water and let rest for 3 days.

The distance between C1 and C4', which are the carbons engaged in the photopolymerization process (1,4'-addition), is 4.00 and 3.71 Å in the asymmetric cell, the packing distance d between monomer units is averaged at 4.78 Å and the angle ϕ between the diacetylene rod and the stacking axis is 59° (see Figures S3, S4, S5a and Table S1 for crystallographic data and structure refinement details). According to the model proposed by Enkelmann in 1984, the essential requirements for efficient polymerization are satisfied.[33] The packing distance is surely affected by the presence of H-bonds between oxygens and hydrogens of the urethane moiety as common in BCMU structures,[30] with two characteristic lengths in the asymmetric cell of 1.93 and 2.03 Å (Figure S5a). Interestingly, on the other side of the diacetylenic unit, tetrazines do not interact by π-stacking and are tilted by 69.20° (Figure S5b), weakening the packing tightness. The C12 alkyl chains are linear and lay on planes tilted by 76.98° (Figure S5c).

2.5 Thin film preparation and morphology

All the macroscopic study presented in this section as well as the nanoscale study presented in the next one were performed on vacuum evaporated diacetylene thin films. Different alternative deposition methods and substrates also give good quality thin films. **TzDA1** can be indeed deposited by spin coating (1000 rpm, 2 min) from a 2 mM solution in MeCN on either glass, ITO or silicon substrates to form films that polymerize efficiently and macroscopically respond to forces, as proven by the spectra shown in Figure S17. The study here presented was however performed on vacuum evaporated thin films. A known amount of powder is introduced in a quartz crucible, which is placed in a high vacuum chamber ($2 \cdot 10^{-5}$ mbar) on top of which, clean microscope slides are fixed. When a stable pressure is reached, a 10°C·min^{-1} temperature ramp is applied, the powder sublimates and the vapor condensates on the glass slides which are at ambient temperature. A 4°C·min^{-1} temperature ramp is applied from the moment the deposition begins until the deposition rate reached the maximal value of 2 Å·s^{-1}. The temperature was manually adjusted to keep the deposition rate as constant as possible. The thickness of the obtained films was measured (when possible) by AFM and is 80 ± 12 nm for 12 mg of **TzDA1** and 313 ± 20 nm for 20 mg of **DA1** (see Supporting Information for details). AFM morphology images of **TzDA1** and **DA1** thin films before (2a and 2c respectively) and after (2b and 2d respectively) photopolymerization are shown in Figure 2. In both cases, rod-shaped crystals lay on a continuous film of deposited diacetylene and this same morphology is found in different zones of the same sample. The statistical distributions of crystal length and width are shown in Figure S6a and S6b respectively; distribution of the crystal orientations for the two samples are shown in Figure S7a (**TzDA1**) and S7b (**DA1**). When looking at the size-distributions, **DA1** films form long and large surface crystals that can often exceed 1 µm length and 400 nm width, whereas most of surface crystals are much smaller for **TzDA1** films, ranging in the 160 – 880 nm interval (in length) and 80 – 240 nm (in width). Moreover, **DA1** surface crystals orientate in specific directions, forming visible domains, as shown in Figure S7b. The photopolymerization, performed under the microscope, does not affect the morphology in accordance with the topotactical polymerization model mechanism.[33,34] Even though the position and dimensions of the crystals are retained in the polymer films, when **DA1** films are exposed to high power UV light or long irradiations, the film cracks along the domains (see Figure 2d, green arrows). The insets are detailed morphology images in smaller scales of the white square areas, and show more clearly that surface crystals do not change either in position or in dimension.

Vacuum evaporated thin films of **TzDA2** show instead a very different morphology. AFM images before (Figure 2e) and after (Figure 2f) photopolymerization show that the compound does not form well-defined crystals. The introduction of an ester function in the self-assembling group results thus in wide arranged aggregates, spaced by empty zones. This inhomogeneous morphology prevents accurate thickness measurements, which could only be estimated by optical UV-Vis absorbance measurements around 80 nm (see SI for details) for 12 mg of **TzDA2** powder. Despite their morphology, polymerization was still effective on these samples, as detailed in section 2.6.

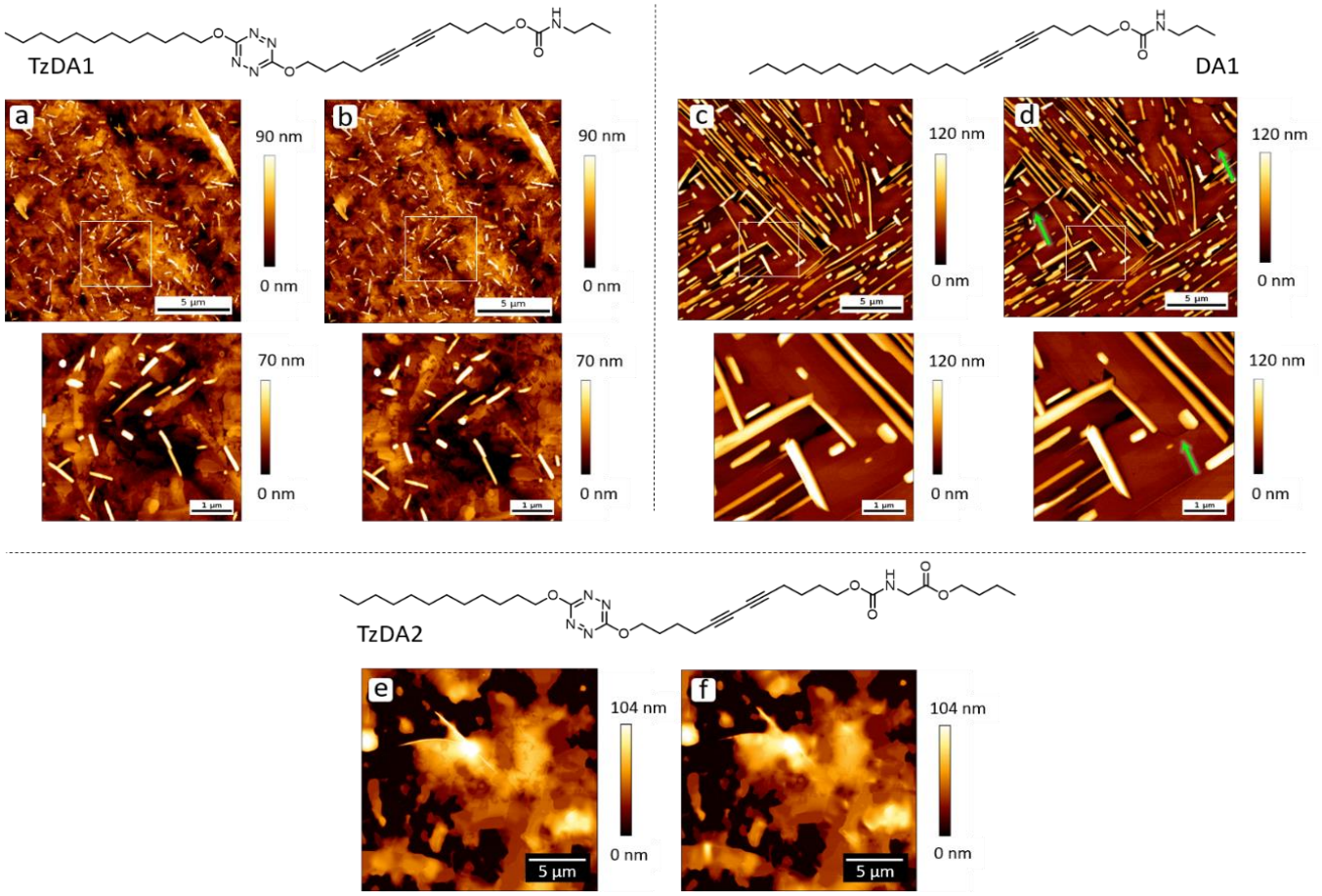

Figure 2. AFM morphology images of TzDA1, DA1 and TzDA2 before (2a, 2c and 2e respectively) and after (2b, 2d and 2f respectively) photopolymerization performed under the microscope at $1.3 \cdot 10^{-4}$ W·cm^{-2} for 70 min on TzDA1 and TzDA2 and 30 s on DA1. The green arrows show the cracks on DA1 films issued by the photopolymerization process.

2.6 Photopolymerization

Self-assembled, crystalline or simply ordered diacetylenes are well known to polymerize in the solid state when irradiated in the UV at 254 nm. However, the kinetics of polymer formation and the total polymer quantity can vary quite a lot according to the specific chemical structure, which in its turn determines a specific supramolecular arrangement and film morphology and eventually influences the response to mechanical stimulations. The capability of one compound to establish intermolecular H-bonds between monomer units is crucial in determining the molecular packing and morphology, and to ensure the minimal distance between reactive centers to favor polymerization, as confirmed by the crystal structure of **TzDA1** shown in section 2.3.

To track the polymerization progress by spectroscopy, a UV-Vis spectrum is recorded after each subsequent irradiation at 254 nm and to each the initial spectrum is subtracted to exclude the contribution of thermally polymerized PDA and tetrazine absorption band in **TzDA1** and **TzDA2** (Figure 3). The thin films are prepared in the same conditions as in Section 2.5. When looking at the spectral shape of the three solid films (Figure 3a for **DA1**, 3b for **TzDA1** and 3c for **TzDA2**), it is confirmed that the presence of tetrazine and the self-assembling group result in different supramolecular arrangements. **DA1**, when irradiated at 254 nm, shows an increase of the absorption band centered at 635 nm and a vibronic band centered at 580 nm, corresponding to the "classical" blue PDA form (light blue arrow in Figure 3a). [11,35] After 14 s of irradiation at 0.33 mW·cm^{-2} (4.62 mJ·cm-2) a progressive distortion of this band towards the low energies (650 nm) is witnessed (see dark blue arrow in Figure 3a). In addition, from 6 mJ·cm^{-2} irradiation energy, a distortion of the band in the low wavelengths is witnessed and is more pronounced for the final steps of the irradiation (high polymer content), leading to a large absorption band covering the range 450 – 650 nm at the end of the polymerization process. This is due to the production of red-poly-**DA1** chains, as it is common to PDAs with fast polymerization kinetics.[36] On the other hand, the photopolymerization of **TzDA1** and **TzDA2** begins with a large and less structured absorption band centered at 600 nm along with the vibronic band at shorter wavelength. This high-energy form is what in literature is referred to as "purple form". [11,12,37] Along the UV irradiation, the band increases and progressively shifts towards higher energies, starting at 196 mJ·cm^{-2} in **TzDA1** and at 38.5 mJ·cm^{-2} in **TzDA2** (see Figure 3b and 3c respectively). This effect could be due to the formation of a new PDA form that coexists with the already present "purple" chains, or to a conversion of the "purple" chains to a new PDA form by plastic deformations

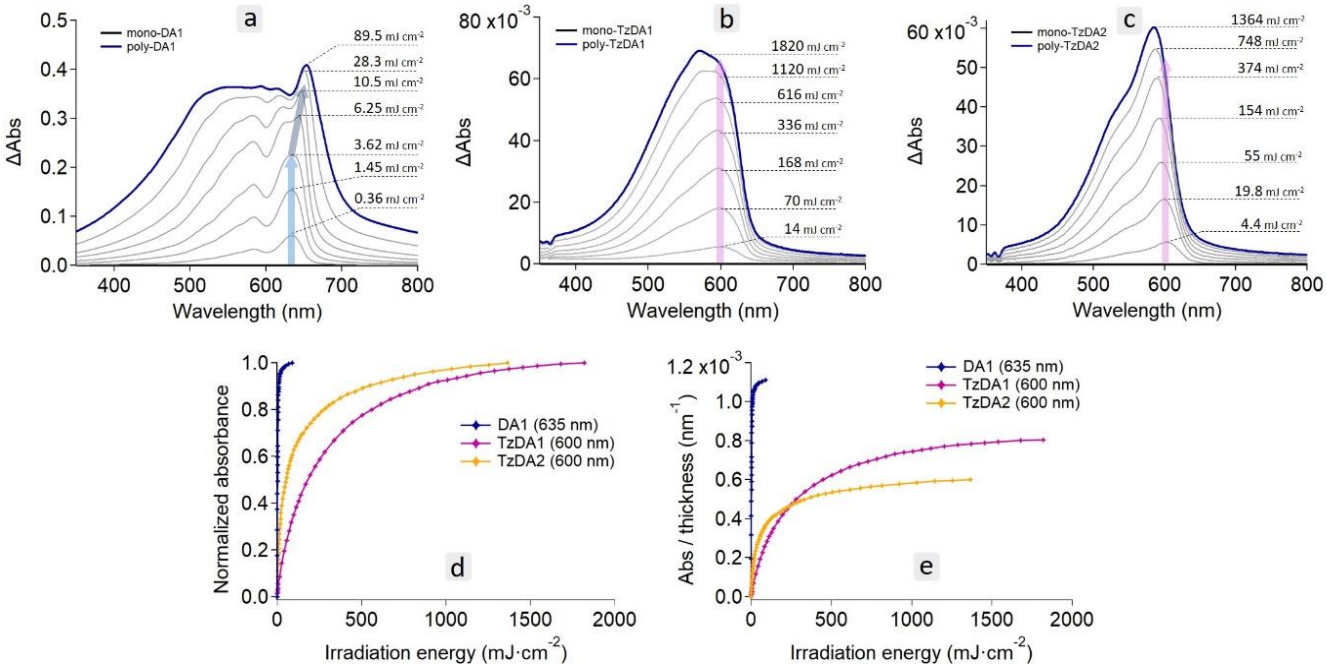

Figure 3. Absorption spectra after subsequent irradiations at 254 nm of thin films of **DA1** (313 ± 20 nm thick), P_{254} = 0.33 mW·cm^{-2} (**a**); **TzDA1** (80 ± 12 nm), P_{254} = 1.4 mW·cm^{-2} (**b**); **TzDA2** (around 80 nm thick), P_{254} = 0.35 mW·cm^{-2} (**c**). Photopolymerization evolution of **DA1**, **TzDA1** and **TzDA2**. Kinetics of the blue polymer formation (**d**), plot of the normalized absorbance of the blue polymer form versus the irradiation energy; total blue polymer quantity that is formed (**e**), plot of the absorbance of the blue polymer normalized by the thickness of the film versus the irradiation energy.

of the polymer film along polymerization. It is however impossible to confirm with certainty one of the two hypotheses from steady state absorption spectra. **TzDA2** shifts sooner than **TzDA1** but shows a smaller shift in the final polymer form of 16 nm (λ_{final} = 584 nm) against the 30 nm witnessed in **TzDA1** (λ_{final} = 570 nm).

Blue polymer formation kinetics can be analyzed and compared looking at the evolution of the normalized blue polymer absorption band versus irradiation energy. The curves obtained for the three compounds are superimposed in Figure 3d. It has to be noted that the total irradiation energy is different for each compound because the irradiation was stopped when a plateau is reached: the last point in the kinetics curve corresponds to the maximum blue polymer quantity that the compound forms in these conditions. It is clear then that **DA1** polymerizes faster than the tetrazine-substituted DA derivatives, since it reaches the maximum blue polymer quantity (at λ_{abs} = 635 nm) with only 90 mJ·cm^{-2}, while **TzDA1** and **TzDA2** (λ_{abs} = 600 nm) require 1.8 and 1.4 J·cm^{-2}, respectively. Therefore, the presence of tetrazine in the structure probably perturbs the efficient packing of DA simple chains which undergo fast and easy photopolymerization. The self-assembling group also plays a role, resulting in a slower photoinduced polymerization for a simple urethane moiety in **TzDA1**. The ratio of blue polymer absorption and film thickness versus the irradiation energy gives a mean to compare the maximum amount of blue polymer formed by UV irradiation. The curves are traced in Figure 3e, where the maximum amount of formed blue polymer is represented by the height of the plateau. Therefore, **DA1** approximately forms two times more blue polymer than **TzDA2** and almost 1.5 times more than **TzDA1**, meaning that the presence of the tetrazine not only slows down the polymerization rate, but also reduces the total amount of polymer formed. Concerning the self-assembling group in tetrazine-substituted derivatives, the simple urethane of **TzDA1** resulted in a globally slower photopolymerization, but in a higher monomer-to-polymer conversion. It is important to highlight that the maximum polymer fraction is far to be 100% for any polydiacetylene, as utterly explained in [38]. In fact, if we assume an absorptivity coefficient α = 3 ± 0.5 x10^5 cm^{-1} for a generic polydiacetylene chain, which is an estimation that allows us to determine an order of magnitude of the amount of polymer formed, the monomer-to-polymer conversion ratio is 6.3 ± 1.1 % for **TzDA1** and 4.9 ± 0.8 % for **TzDA2**. Assuming the same absorptivity coefficient, a conversion ratio of 9.2 ± 1.5 % is obtained for **DA1**. When looking at the evolution of the spectral shape of the subsequent absorption spectra of **DA1** photopolymerization (Figure 3a), it is clear that such an analysis does not take into account the whole complexity of the system. In fact, this estimates only the quantity of one blue polymer form, excluding the 650 nm form and the red-poly-**DA1**.

2.7 Fluorescence and energy transfer

The progress of photopolymerization of **DA1** thin films cannot be directly followed by fluorescence spectroscopy since the blue phase of the polymer is non-fluorescent. When the polymerized film is heated on a heating plate at around 80°C, the blue to red conversion activates the fluorescence of the system (absorption and fluorescence spectra in Figure S8). The fluorescence quantum yield in the solid state was measured by means of an integrating sphere

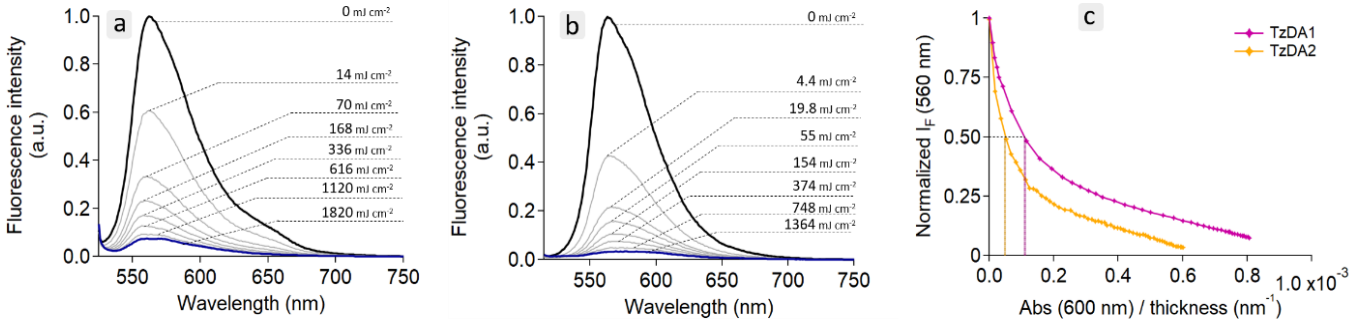

Figure 4. Fluorescence spectra after subsequent irradiations at 254 nm of thin films of TzDA1, P_{254} = 1.4 mW·cm^{-2}, λ_{exc} = 510 nm (a); TzDA2, P_{254} = 0.35 mW·cm^{-2}, λ_{exc} = 500 nm (b). Correlation of normalized fluorescence intensity with blue polymer relative absorbance (Abs(600nm)/thickness) of TzDA1 and TzDA2 for progressive irradiation at 254 nm (c).

and is less than 1%, which is more reliable than the value of 2-3% obtained by means of comparison to a standard fluorophore dissolved in nail polish and painted on a glass slide. [31] These values are consistent if we consider that solid state measurements performed at 15 and 40K gave 0.30 ± 0.05 and 0.20 ± 0.05 respectively, showing a decrease of φ_F with temperature. [39] At low temperatures, the fluorescence lifetime is fitted by a single exponential function with τ = 94 ps, which becomes shorter with increasing temperature. [40] In fact, the fluorescence lifetime of **DA1** thin films at room temperature was found to be shorter than 10 ps, according to the instrument resolution. Inserting a tetrazine in the chemical structure is therefore a valuable strategy to ameliorate the emission properties of the system (higher quantum yield and longer fluorescence lifetime).

Tetrazine fluorescence in **TzDA1** and **TzDA2** is modulated accordingly with the state of the chain. The tetrazine chromophore is highly fluorescent in monomeric form (ON state), quenched when the DA is polymerized to the blue form (OFF state) and recovers the emission when the polymer is stimulated (thermally or mechanically) and converted to the red form (ON state). It is possible to follow the emission quenching by steady-state fluorescence spectroscopy, recording a spectrum after subsequent irradiations at 254 nm which gradually polymerize the thin films (Figure 4). As it can be noticed, the tetrazine fluorescence spectral shape is not affected by the photopolymerization process, but the intensity only is quenched. When photopolymerization is achieved, 91% of the initial tetrazine fluorescence is quenched in poly-**TzDA1** (Figure 4a), and 94% in poly-**TzDA2** (Figure 4b).

To evaluate the tetrazine quenching efficiency by poly-**TzDA1** and poly-**TzDA2** along the photopolymerization reaction, the maximum of fluorescence emission (560 nm) is plotted as a function of the UV-vis absorption at 600 nm divided by the film thickness for the two samples, corresponding to the amount of blue polymer formed. The curves are shown in Figure 4c.

In both samples, the decrease in fluorescence emission is faster than the increase in absorption at 600 nm, resulting in a non-linear correlation proving an efficient energy transfer from multiple tetrazine donors to blue-PDA acceptor. The dotted lines in Figure 4c underline how the efficiency in Tz-quenching is more pronounced in **TzDA2** than in **TzDA1**, showing that 50% of fluorescence quenching is reached for a lower blue polymer quantity (lower blue-PDA absorption) in **TzDA2**. In absolute terms, an extraordinary energy transfer efficiency is achieved in both systems, where less than 2% of blue-PDA suffice to quench the fluorophore fluorescence signal by 50% of its initial intensity. Since the energy transfer processes are strongly driven by spatial parameters (distance and relative orientation between the emitter and the quencher species), the different fluorescence quenching profiles of **TzDA1** and **TzDA2** as a function of photopolymerization conversion (Figure 4c) is a strong indication that the supramolecular arrangement of the tetrazine dyes and PDA molecules, as well as the polymerization distribution within the material, are not identical for the two compounds.

To investigate the dynamics of the energy transfer processes upon photopolymerization, fluorescence decay curves and solid state fluorescence quantum yields for subsequently UV-irradiated films (same vacuum evaporated films used for steady-state spectroscopy measurements) of **TzDA1** were recorded. The monomer in CH_3CN solution presented in Figure S9 shows the typical profile of a tetrazine fluorescence decay, with a mean lifetime of 35.6 ns (see table S2 for a summary of the photophysical properties of **TzDA1**, **TzDA2** and **DA1**). [41] The decay profiles of progressively polymerized thin films are shown in Figure 5a and the corresponding fluorescence steady-state spectra in Figure S12a. The fluorescence decays would require multiple discrete exponentials to obtain satisfactorily fits. The physical meaning of such multiexponential discrete functions is questioning in the present case, and we decided to use a sum of a stretched and a discrete exponential (equation 1) to model the experimental fluorescence decay profiles of **TzDA1**:

$$I(t) = a_1 \cdot exp\left[-\left(\frac{t}{\tau_1}\right)^{\beta}\right] + a_2 \cdot exp\left(\frac{t}{\tau_2}\right) \qquad \text{(equation 1)}$$

performing a global analysis where the discrete component was fixed for all the decays, while the stretched component was left free. The stretched exponential [42,43] can efficiently reflect an underlying distribution of time-decays in such a complex (heterogeneous) system, evolving with the

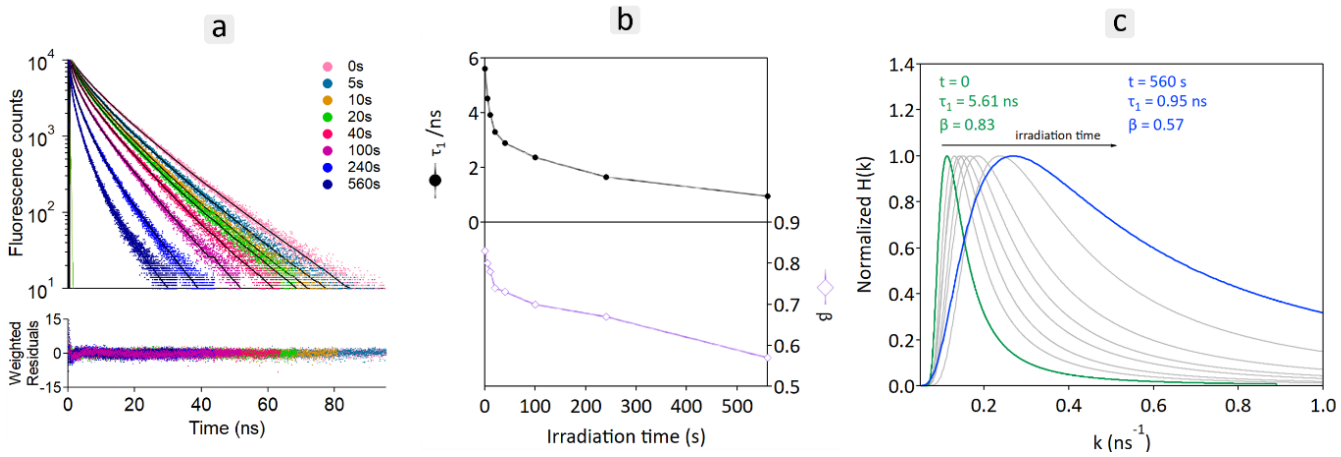

Figure 5. Lifetime profiles of progressively photopolymerized thin films of **TzDA1** (**a**); evolution of the stretched exponential fitting parameters τ_1 and β as a function of irradiation time (lines are a guide to the eyes) (**b**); rate constant distribution for each polymerization step (**c**).

irradiation time, whereas the discrete component can take into account a minor emissive contribution which stays constant under irradiation. The global χ_R^2 of the analysis is 1.17. The fitting parameters are shown in the table in Figure S12b. The discrete decay-time was determined at 0.22 ns. Along polymerization, the tetrazine lifetime is expected to decrease progressively because of energy transfer to increasing quantities of acceptor (blue-poly-**TzDA1**), which is what qualitatively can be concluded from Figure 5a, with a progressive shortening of the fluorescence decays upon UV irradiation. As shown in Figure 5b, the stretched exponential parameters τ_1 and β decrease with increasing irradiation time (increasing quantity of blue-poly-**TzDA1**), which qualitatively represents a shortening and a widening of the overall decay-time distribution. Indeed, the stretched exponential that is used to fit the fluorescence decay profile I(t) can be treated as a distribution of rate constants H(k) as expressed by the following equation:

$$I(t) = \int_0^\infty H(k)e^{-kt}dk \qquad \text{(equation 2)}$$

H(k) being the inverse Laplace transform of I(t). The normalized distributions of decay rates were obtained from a mathematical treatment described by M.N. Berberan-Santos et al., [44] and the corresponding H(k) curves are shown in Figure 5c. They reveal a progressive shortening of the decay time along the polymerization process: at 0s irradiation time, k is comprised between 0.05 and 0.2 ns^{-1} (5-20 ns decay time), while at 560s irradiation time, the k distribution is much larger, comprised between 0.1 and 2 ns^{-1} (0.5-10 ns decay time). To confirm that the fluorescence quenching mainly corresponds to a quenching of the stretched component, it is necessary to evaluate the intensity fractions of the discrete and stretched components in the overall decay function and their evolution with UV irradiation time. Figures S13a-b show the plots of the total exponential function (sum of the two components) and the single stretched and discrete components of 0 s and 560 s irradiations respectively. The ratio of the numerical integration of the single components (stretched exponential and discrete exponential, respectively) and the integration of the total exponential function gives a relative fraction of intensity (f stretched and f discrete), underlining that the discrete component has a minor (<4%) contribution to the overall fluorescence emission. The sum of these values is then normalized to the steady-state fluorescence intensity. The table in Figure S13c sums up all the values (f stretched and discrete, normalized or not), and Figure S13d displays the evolution of the normalized intensity fraction of the stretched exponential with irradiation time, confirming that fluorescence quenching mainly corresponds to a quenching of the stretched component.

Therefore, the long stretched component is assigned to the tetrazine fluorophores that are involved in the energy transfer to the blue-poly-**TzDA1**, with a wide distribution of efficiencies. On the other hand, the short discrete component could represent a small portion of the tetrazine that has been degraded, probably during vacuum evaporation, and does not take part in the quenching mechanism, with a larger relative contribution at longer irradiation time, when the tetrazine fluorophores are quenched in larger extents (Figure S13d).

An ulterior proof of the energy transfer mechanism is constituted by the fluorescence quantum yields that were calculated on the first and last step of the photopolymerization process, by means of an integrating sphere. It was found for the monomeric film φ_F = 17.3%, while for the polymeric film φ_F = 1.2%.

2.8 Nanoscale mechanofluorochromism

The responsiveness of **DA1** and **TzDA1**[26] was first of all tested at the macroscale by UV-Vis spectroscopy (vacuum evaporated thin films on glass slides) and steady-state fluorescence spectroscopy (drop-casted films on paper substrate, to avoid material loss while scratching) by applying a mechanical friction with a spatula. The absorption spectra before and after mechanical stimulation of **DA1** (Figure S14a) and of **TzDA1** (Figure S15a) show that both compounds convert from the blue to the red form of the

polymer upon mechanical stress with the disappearing of the blue phase absorption band at 635 (**DA1**) and 600 nm (**TzDA1**) and increasing of the red phase absorption band at 540 nm. Consistently, a fluorescence activation is witnessed when blue-poly-**DA1** is stimulated and converted to red-poly-**DA1** (red curve in Figure S14b) and tetrazine's fluorescence signal is restored in **TzDA1** (red curve in Figure S15b). In order to test and quantify the fluorescence response at the nanoscale to mechanical forces of these compounds, an atomic force microscope coupled with a fluorescence microscope was used.[26,45] The AFM was set in contact mode to apply a mechanical friction to the thin film with a well-defined vertical force component and the fluorescence microscope probed the fluorescence modification before and after shearing of the same zone. Squared 3x3 µm scans were performed in contact mode ranging the vertical force from 20 to 600 nN at the constant scan rate of 6.1 $\mu m \cdot s^{-1}$. Each squared stimulated area thus corresponds to a stimulation of well-defined force. **TzDA1** and **TzDA2** recover their fluorescence that has been quenched by polymerization (tetrazine ON-to-OFF-to-ON), while **DA1** simple chain is a pure OFF-to-ON system, relying on the intrinsic fluorescence of polydiacetylene red chains resulting from the stimulation.

DA1 presents a different morphology that leads to a different response to mechanical stimuli compared to **TzDA1**. Morphology and fluorescence images of non-emissive blue-poly-**DA1** (obtained by 70.4 s irradiation at 254 nm with an irradiation power of $7.2 \cdot 10^{-5}$ $W \cdot cm^{-2}$) are shown in Figure 6a and b. The irradiation time and power were adjusted to have a comparable amount of polymer in the two films (**DA1** = 7.0 ± 1.2%; **TzDA1** = 5.4 ± 0.9%). In Figure 6c, the morphology image of the same zone after mechanical stimulation is presented, and the specific scratched areas are highlighted by white dashed squares. Vertical force was varied from 25 to 300 nN and the corresponding fluorescence image is shown in Figure 6d. Subtraction of images after and before the stimulations allows to suppress the background signal and to examine the fluorescent signal coming from the blue-to-red conversion only. A numerical value of this signal can be obtained by integrating over the sheared area and can be plotted versus the vertical applied force to build a fluorescence-force correlation curve. Indeed, poly-**DA1** and poly-**TzDA1** are both converted to a fluorescent state when sheared by an AFM tip. When this procedure is performed systematically on different zones of the samples varying the applied vertical force, the correlation plots between fluorescence activation and applied force are built and displayed in Figure 6e. As already reported in our previous work, [26] the fluorescence signal of the tetrazine dye is clearly increasing along with the level of vertical force applied to the sample by the AFM tip during the friction, until a plateau is reached around a nominal vertical force of ~200 nN (Figure 6e, black dots). Under our experimental conditions, the fluorescence restauration observed at this plateau is slightly higher than the one observed by manual shearing at the macroscale (see figure S15b and S22). In the case of poly-**DA1**, the fluorescence signal is also increasing under AFM-based mechanical trigger. However, this tendency is not as straightforward as it was found for poly-**TzDA1** (Figure 6e, blue triangles). Taking into consideration (i) that **DA1** thin films are 4 times thicker than **TzDA1** films thus absorb 3 times more at the excitation wavelength (488 nm), (ii) the irradiation power and time were adjusted to reach a comparable polymerization extent, and (iii) that the resulting fluorescence signal upon mechanical stimulation is 7-fold lower for **DA1** than **TzDA1**, we can conclude that the introduction of the tetrazine fluorophore accounts for most of the fluorescence activation enhancement at the plateau. Attenuation through the film of excitation light and fluorescence reabsorption phenomena can be reasonably neglected since the absorption at these wavelengths is lower than 0.1. When a vertical force only is applied on blue-poly-**TzDA1** films, no fluorescence recovery is registered in the area, as shown in Figure S20, suggesting that a friction force is required to induce the blue-to-red polymer conversion. [46] Compared to poly-**TzDA1**, poly-**DA1** thin films are less deformable. If in the former forces higher than 200 nN deeply perturb the film surface morphology, vertical forces up to 600 nN do not seem to affect noticeably the surface topology of poly-**DA1** thin films (see Figure S18). The resistance to deformation results in a mild fluorescence recovery comprised in a short range of fluorescence integration values, and is probably due to a tighter packing of the polymer chains, which result in a globally stiffer film. External factors may also influence the efficacy of mechanical stimulations. An important factor that comes into play in these experiments is the quality of the AFM tip after one or more stimulations. In fact, the friction between the tip and a stiff sample surface like poly-**DA1** can deform it, while in softer films like poly-**TzDA1** some material can be detached from the sample surface and stick to the tip. When the AFM tip is deformed, damaged or polluted, the correlation between applied vertical force and the actual mechanical stress experienced by the sample is reduced. This may explain why in the same experiment it is not rare to witness a milder morphological change for consecutive increasing mechanical stimulations, as it can be seen in Figure 6, where vertical forces of 125 – 200 nN seem to impact less the morphology (6c) and cause a milder fluorescence activation (6d) compared to vertical forces of 25 – 100 nN.

Therefore, the presence of the tetrazine is advantageous in two ways for this kind of application. Firstly, it increases the OFF-to-ON contrast of the system, making detection easier and instrumental error less impacting. Secondly, its presence untightens the packing between polymer chains, leading to a softer film whose deformation and fluorescence recovery is well-correlated to the intensity of the applied mechanical force, as observed for poly-**TzDA1**, which is a quite promising characteristic for sensitive and quantitative mechanical sensors.

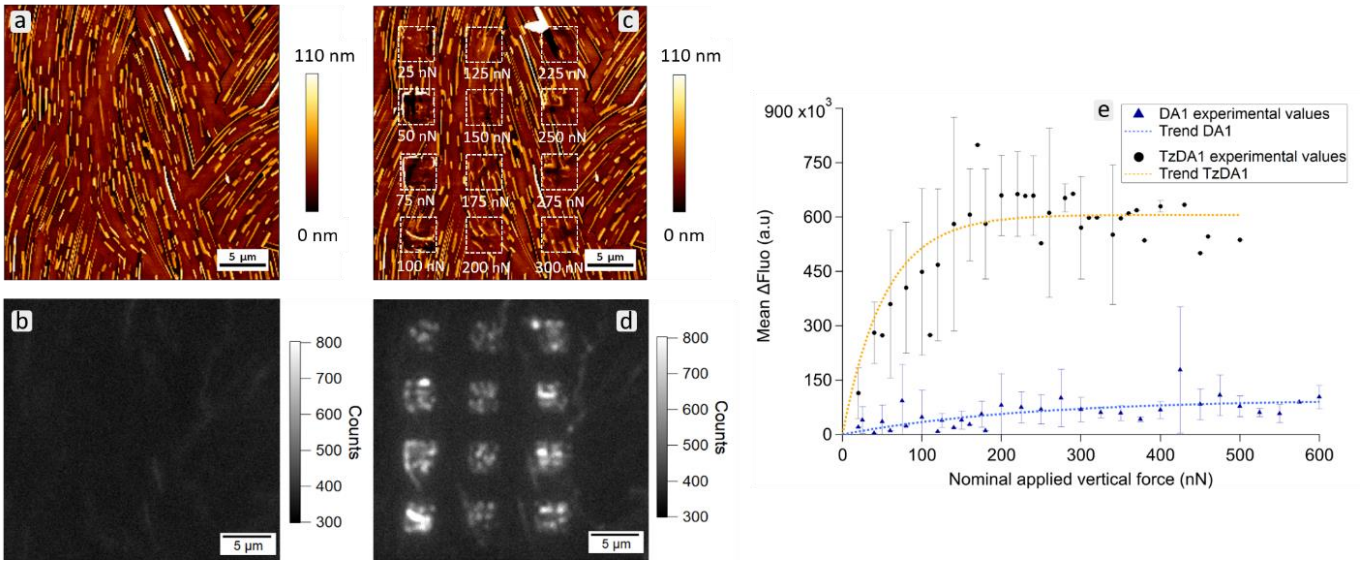

Figure 6. Morphology (a, c) and corresponding fluorescence images (b, d) (λ_{exc} = 488 nm) of **DA1** thin films before (a, b) and after (c, d) mechanical stimulation. Each area was scanned from bottom to top with forces ranging from 25 to 300 nN at a tip velocity of 6.1 µm·s^{-1} (forward scan: left to right; return scan: right to left). Graphical representation (e) of the fluorescence signal in each scraped area versus the corresponding applied vertical force for **DA1** (blue triangles) and **TzDA1** (black dots). Each point corresponds to the mean value of mechanical stimulations in different areas of the same sample (complete list of measurement can be found in Table S3 and S4 for **DA1** and **TzDA1** respectively), and the error bars correspond to the standard deviation. The orange and blue dotted lines are the generic trends that are found in **TzDA1** and **DA1** respectively, and they are used as guides to eye.

In this regard, the self-assembling group plays also an important role. It is shown in section 2.6 how **TzDA2** photopolymerizes faster but forms globally less blue polymer than **TzDA1**. Nonetheless, poly-**TzDA2** quenches the tetrazine fluorophore more efficiently, as shown in section 2.7, which is expected to result in a wider range of forces that can be probed. Mechanofluorochromism was evidenced at the macroscale as shown in the spectra in Figure S16, and cycles of irradiation-mechanical stimulation highlight a pseudo-reversible response to mechanical stress as observed for **TzDA1**[26] but the resulting inhomogeneous morphology is not well adapted to the experiments at the nanoscale shown in this work, whose reproducibility depend on the homogeneity of the sample surface, that ensures the possible comparison between different stimulated areas. Figure S19 shows AFM images of poly-**TzDA2** before (19a) and after (19c) mechanical shearing and their corresponding fluorescence images (19b and 19d respectively). Vertical applied force was varied from 180 to 340 nN in 9 different areas. The ones corresponding to 200, 240 and 260 nN were not as morphologically affected as the others and as a consequence they do not restore as much the fluorescence. When looking at the corresponding morphology before stimulation (Figure S19a), these areas do not present a homogeneous crystalline surface, but just small aggregates laying on the substrate, as highlighted by the green dotted lines. Blue dotted lines show instead that the areas where fluorescence recovery was stronger are laying on crystalline aggregates. Therefore, applications of poly-**TzDA2** are still worth considering in different aggregation states (like isolated microcrystals), leaving, up to now, poly-**TzDA1** the best adapted compound to probe friction forces in the nN range on thin films.

3. Experimental section

Synthesis

All reagents were purchased from commercial supplier, and used without further purification. Anhydrous solvents were dried and purified by passage through alumina columns. All reactions were monitored by Thin Layer Chromatography (TLC) using E Merck TLC silica gel 60 F254, thickness 0.2 µm, and visualized under UV 254 nm or $KMnO_4$ revelation. ^{1}H and ^{13}C NMR spectra were recorded on a JEOL JMS ECS 400 MHz spectrometer (100 MHz for 13C) at 25°C. Chemical shifts are expressed in ppm and defined in respect to TMS = 0 ppm for ^{1}H and ^{13}C. The following abbreviations are used to describe the signals: s for singlet; d for doublet; t for triplet; q for quadruplet; m for multiplet. High resolution mass spectrometry was performed at the CNRS Imagif platform. Melting points were measured with a Stuart apparatus SMP10.

X-ray diffraction

X-ray diffraction data for compound **TzDA1** was collected by using a VENTURE PHOTON100 CMOS Bruker diffractometer with Micro-focus IuS source Cu Kα radiation. Crystals were mounted on a CryoLoop (Hampton Research) with Paratone-N (Hampton Research) as cryoprotectant and then flashfrozen in a nitrogen-gas stream at 100 K. For compounds, the temperature of the crystal was maintained at the selected value by means of a N-Helix Cryostream cooling device to within an accuracy of ±1K. The data were corrected for Lorentz polarization, and absorption effects. The structures were solved by direct methods using SHELXS-97 [47] and refined against F2 by full-matrix least-squares techniques using SHELXL-2018 [48] with anisotropic

displacement parameters for all non-hydrogen atoms. Hydrogen atoms were introduced into the calculations as a riding model with isotropic thermal parameters. All calculations were performed by using the Crystal Structure crystallographic software package WINGX. [49] The crystal data collection and refinement parameters are given in Table S1. [CCDC 2010463 contains the supplementary crystallographic data for this paper. These data can be obtained free of charge from The Cambridge Crystallographic Data Centre via www.ccdc.cam.ac.uk/data_request/cif.]

Steady-state spectroscopy

The UV/Vis absorption spectra were recorded on a double beam spectrophotometer Cary 5000 from Agilent Technologies equipped with deuterated/halogen lamps. The emission spectra were recorded on the Fluorolog FL3-221 from Horiba Jobin-Yvon with xenon light source.

Irradiation at 254 nm was performed by a Hg/Xe LC8 – Lightningcure (200 W) light source from Hamamatsu. An interferential filter from Semrock is added to select the 254 nm mercury line. The power of the irradiation was calculated with an Ophir powermeter (PD300-UV), using a Schott long pass filter (LP) 385 nm to measure the residual infrared light that is let through the Semrock filter, considering a 90% transmittance of the LP filter:

$P_{254} = TotalPower - [{}^{10}/_{9}\,(PowerLP385)]$. (equation 3)

Solid state photoluminescence quantum yield

Absolute solid state φ_F were obtained by means of a Quanta-ϕ F-3029 integrating sphere by Horiba scientific. Fluorescence was excited at 360 nm in **TzDA1** and at 488 nm in DA1. The ratio of emitted and absorbed photons (quantum yield) was obtained using the calculation sheet provided by the constructor. The error on the quantum yield is estimated to ±10%.

Time-resolved spectroscopy

Emission lifetime measurements were performed via Time-Correlated Single Photon Counting (TCSPC) method. Excitation was done via Titanium:Sapphire femtosecond oscillator laser (Tsunami, Spectra Physics) pumped by a double intra-cavity Nd:YVO4 laser (Millenia Xs, Spectra Physics). The wavelength was adjusted at 720 nm at the output of the oscillator. Repetition rate was reduced to 4 MHz by a pulse selector (model 3980, Spectra Physics). The wavelength at 360 nm was generated by focalizing the fundamental beam at 720 nm inside a nonlinear SHG crystal. The pulse duration of the excitation laser at 360 nm was less than 500 fs. The emission was detected perpendicular to the excitation beam through a low pass filter (to remove the excitation light), an analyzer at magic angle, a monochromator, and a MCP-PMT detector (R3809U-50, Hamamatsu) connected to a TCSPC card (SPC 630, Becker & Hickl). The instrumental response function was recorded for each decay curve. The data were analyzed with multiexponential functions including reconvolution analysis, using the Globals software (Laboratory for Fluorescence Dynamics at the University of California, Irvine).

Microscopy

Coverglass cleaning

The coverglasses were preliminary cleaned before film deposition by several steps of sonication in the following solvents: 1% Hellmanex water solution, acetone, ethanol, 1M sodium hydroxide water solution and distilled water, then dried with a heat gun.

Vacuum evaporation protocols

The deposition of thin films was carried out using a Leybold Univex 300 vacuum evaporator. The pure organic powder obtained from the synthesis was introduced in the crucible (20 mg of **DA1**, 11.2 mg of **TzDA1**, 12 mg of **TzDA2**) and thin films were obtained. The crucible, placed in a vacuum chamber ($2{\cdot}10^{-5}$ mbar), was heated by means of a tungsten filament source and the temperature was controlled by a thermocouple.

DA1. A heating rate of 4°C·min^{-1} was used from 25 to 80°C, and when the deposition rate approached 0 Å·s^{-1} the furnace temperature was increased to 90°C with a 4°C·min^{-1} heating rate.

TzDA1. A heating rate of 10°C·min^{-1} was used from 25 to 120°C. Then the rate was reduced to 4°C·min^{-1} from 140-160°C. When the temperature reached 160°C, the speed of deposition was manually controlled to be 2 Å·s^{-1} maximum by adjusting the furnace temperature.

TzDA2. A heating rate of 4°C·min^{-1} was used from 25 to 170°C, temperature that was kept constant until the end of the deposition.

Film thickness and growth rate were monitored in situ by a piezoelectric quartz crystal system. Film thickness was measured by manually performing a scratch and measuring the step height by AFM in 5 different points along the scratch.

The microscopy set-up

The microscopy set up is composed by an optical microscope (Nikon, Eclipse Ti-U) on which an AFM microscope (JPK NanoWizard®-3) was implemented. The diascopic illumination part was optimized to be UV compatible. An Hg/Xe light source (Hamamatsu, LC8) was used with an interferential filter at 254 nm (Semrock, Hg01-254-25) on this illumination part to make a localized round irradiation on the sample of around 2 mm². During irradiation at 254 nm, the AFM head was removed in order to have a homogeneous irradiation zone.

Fluorescence pictures were recorded in epifluorescence mode. LED light source at 488 nm (Lumencor, Spectra X) was focused on the sample via a dichroic filter set (Semrock, LF488/LP-B-000) and a microscope objective (Nikon, 60X/0.95 ON Plan Apo λ). Emission signal was directed to an EMCCD camera (Andor, iXon Ultra 897) working in CCD mode.

Topography AFM images were recorded in QI mode with a cantilever with nominal spring constant of 7.4 N·m^{-1}

(Nanosensors, PPP-NCSTR). Mechanical frictions were done in contact mode with a silicon cantilever with diamond-like carbon coating of nominal spring constant of 40 $N \cdot m^{-1}$ (Budgetsensors, Tap300DLC). The thermal tune calibration, included in the JPK software, was used to make the calibration of the spring constant. Image analysis was performed using the JPK analysis software. Calibrations and AFM pictures (QI and contact mode) were done under ambient conditions.

Statistical analyses were performed on Figure 2a for **TzDA1** and 2c for **DA1**, using Gwyddion software. Isolated objects were marked by selecting an appropriate threshold, those touching the edges of the image were automatically excluded and those with an area smaller than 3 pixels were not taken into account. This last step leads to the exclusion of small objects of length lower than 250 nm (according to the image resolution, one pixel corresponds to 80 nm).

Conclusions

Two novel diacetylenes molecules, **DA1** and **TzDA2**, analogues of the previously published **TzDA1**, have been synthesized through a 3-steps and 4-steps synthesis respectively. With respect to **TzDA1**, the chemical structure was variated, removing the tetrazine fluorophore in **DA1** and adding a butyl-ester function in **TzDA2**, to evaluate the effect of these variations in the photopolymerization process, fluorophore quenching efficiency and response to mechanical stress at the nanoscale. Vacuum evaporation of these molecules led to thin films with different morphologies, that were studied by atomic force microscopy. Rod-shaped crystals lay on a continuous film of deposited **DA1** and **TzDA1**, that are statistically longer and thicker in the former than in the latter. **TzDA2**, instead, forms wide arranged aggregates, spaced by empty zones. The different spatial arrangement is responsible for the different spectral shapes in the steady-state spectroscopy measurements that were used to track the photopolymerization process, where a well-defined UV irradiation is sent to the film and an absorption and fluorescence spectrum were recorded. **DA1** polymerizes globally more and faster than the other derivatives, but produces different polymer phases that coexist in the film: blue (λ_{abs} = 635 and 650 nm) and red (λ_{abs} = 540 nm). **TzDA1** and **TzDA2** present a well-structured band centered at 600 nm (purple form). **TzDA2** polymerizes faster but globally produces less polymer at the end of the photopolymerization process than **TzDA1**. However, the quenching efficiency of the tetrazine fluorophore by blue-poly-**TzDA2** is more efficient than by blue-poly-**TzDA1**, as shown by steady-state fluorescence spectroscopy measurements. In absolute terms, an outstanding tetrazine quenching efficiency is obtained in TzDAs, since the signal is quenched by 50% of its initial intensity by less than 2% of blue-PDA. Time-resolved fluorescence measurements were performed to shed light on the quenching dynamics of TzDAs for increasing quantities of blue-PDA quenchers. For each polymerization step of **TzDA1**, the decay profile was fitted by the sum of a stretched and discrete exponential components. It was shown that the quenching mechanism essentially corresponds to a quenching of the stretched component, confirmed by a shortening and widening of the decay time distribution, and a decrease of its intensity fraction along polymerization. This long, stretched component thus corresponds to the portion of tetrazine involved in the energy transfer, while the short, discrete component would be a small portion of tetrazine that was degraded during vacuum evaporation and that does not take part to the quenching process. At last, the response to mechanical stress at the nanoscale was tested on the PDAs thin films, using an atomic force microscope coupled to a fluorescence microscope. AFM serves to apply a shear stress and the fluorescence microscope probes the fluorescence activation in the same zone of stress application. It was found that the presence of tetrazine in **TzDA1**, as compared to **DA1**, is crucial in enhancing the fluorescence activation by shear stress, noticeably increasing the emission quantum yield of the system that makes detection easier and instrumental error less impacting. In addition, it untightens the packing between polymer chains, leading to a softer film whose deformation and fluorescence recovery is well-correlated to the intensity of the applied mechanical force, as observed for poly-**TzDA1**. In the future, thin films of poly-**TzDA1** with a well-defined response to mechanical forces could be used to develop microfluidic chips with integrated force sensors, allowing the measurement of shear stress exerted by the flow or by a microobject circulating in the chip.

Author Contributions

Conceptualization: L.P., A.B., R.M., C.A. (equal); Data curation: L.P. (lead), A.B. (supporting); Investigation: L.P. (lead), A.B. (supporting), R.G. (crystallographic data); Methodology: L.P. (lead), A.B., R.M., C.A. (equal); Project administration: L.P. (lead), A.B. (supporting); Resources: A.B., R.M., C.A. (equal); Software: R.M. (lead), A.B. (equal); Supervision: C.A., R.M. (equal); Validation: L.P. (lead), A.B., R.M., C.A. (equal); Visualization: L.P.; Writing – original draft: L.P.; Writing – review & editing: C.A., R.M., A.B. (supporting).

Conflicts of interest

There are no conflicts to declare.

Acknowledgements

This project has received funding from the H2020-EU.1.1. research and innovation programme(s) – ERC-2016-STG under grant agreement No 715757. M. Adrien Smith and Ms Noémie Demurget are acknowledged for technical help with the synthesis of **TzDA2** and **DA1** compounds, Mr J.-F. Audibert and Dr. R. Pansu are acknowledged for the

measurement of the fluorescence lifetime of **TzDA2** thin film.

Notes and references

1 K. Ariga, T. Mori and J. P. Hill, *Adv. Mater.*, 2012, **24**, 158–176.
2 Y. Sagara, S. Yamane, M. Mitani, C. Weder and T. Kato, *Adv. Mater.*, 2016, **28**, 1073–1095.
3 G. Zhang, J. Lu, M. Sabat and C. L. Fraser, *J. Am. Chem. Soc.*, 2010, **132**, 2160–2162.
4 K. Mizuguchi, H. Kageyama and H. Nakano, *Mater. Lett.*, 2011, **65**, 2658–2661.
5 S.-J. Yoon and S. Park, *J. Mater. Chem.*, 2011, **21**, 8338–8346.
6 H. Ito, M. Muromoto, S. Kurenuma, S. Ishizaka, N. Kitamura, H. Sato and T. Seki, *Nat. Commun.*
7 D. Genovese, A. Aliprandi, E. A. Prasetyanto, M. Mauro, M. Hirtz, H. Fuchs, Y. Fujita, H. Uji-I, S. Lebedkin, M. Kappes and L. De Cola, *Adv. Funct. Mater.*, 2016, **26**, 5271–5278.
8 B. R. Crenshaw and C. Weder, *Chem. Mater.*, 2003, **15**, 4717–4724.
9 Y. Chen, C. J. Yeh, Y. Qi, R. Long and C. Creton, *Sci. Adv.*, 2020, **6**, eaaz5093.
10 O. Yarimaga, J. Jaworski, B. Yoon and J.-M. Kim, *Chem. Commun.*, 2012, **48**, 2469.
11 R. W. Carpick, D. Y. Sasaki, M. S. Marcus, M. A. Eriksson and A. R. Burns, *J. Phys.: Condens. Matter*, 2004, **16**, R679.
12 J.-S. Filhol, J. Deschamps, S. G. Dutremez, B. Boury, T. Barisien, L. Legrand and M. Schott, *J. Am. Chem. Soc.*, 2009, **131**, 6976–6988.
13 X. Chen, G. Zhou, X. Peng and J. Yoon, *Chem. Soc. Rev.*, 2012, **41**, 4610–4630.
14 X. Sun, T. Chen, S. Huang, L. Li and H. Peng, *Chem. Soc. Rev.*, 2010, **39**, 4244–4257.
15 S. Lee, J.-Y. Kim, X. Chen and J. Yoon, *Chem. Commun.*, 2016, **52**, 9178–9196.
16 X. Qian and B. Städler, *Chem. Mater.*, 2019, **31**, 1196–1222.
17 R. W. Carpick, D. Y. Sasaki and A. R. Burns, *Langmuir*, 2000, **16**, 1270–1278.
18 S. S. Lee, E. H. Chae, D. J. Ahn, K. H. Ahn and J.-K. Yeo, *Korea-Aust. Rheol. J.*, 2007, **19**, 43–47.
19 H. Feng, J. Lu, J. Li, F. Tsow, E. Forzani and N. Tao, *Adv. Mater.*, 2013, **25**, 1729–1733.
20 S. Chae, J. P. Lee and J.-M. Kim, *Adv. Funct. Mater.*, 2016, **26**, 1769–1776.
21 H. Terada, H. Imai and Y. Oaki, *Adv. Mater.*, 2018, **30**, 1801121.
22 J. P. Lee, H. Hwang, S. Chae and J.-M. Kim, *Chem. Commun.*, 2019, **55**, 9395–9398.
23 M. A. Reppy, *J Fluoresc*, 2008, **18**, 461–471.
24 X. Li, M. McCarroll and P. Kohli, *Langmuir*, 2006, **22**, 8615–8617.
25 T. Barisien, J.-L. Fave, S. Hameau, L. Legrand, M. Schott, J. Malinge, G. Clavier, P. Audebert and C. Allain, *ACS Appl. Mater. Interfaces*, 2013, **5**, 10836–10841.
26 L. Polacchi, A. Brosseau, R. Métivier and C. Allain, *Chem. Commun.*, 2019, **55**, 14566–14569.
27 V. Enkelmann, G. Wenz, M. A. Müller, M. Schmidt and G. Wegner, *Mol. Cryst. Liq. Cryst.*, 1984, **105**, 11–39.
28 A. Prock, M. L. Shand and R. R. Chance, *Macromol.*, 1982, **15**, 238–241.
29 S. Sottini, E. Giorgetti, M. Sparpaglione, D. Brooks, M. Licchelli, D. Grando, V. Skarda and D. Westland, *Opt. Mater.*, 1996, **5**, 285–291.
30 S. Spagnoli, M. Schott, M. Johnson and L. Toupet, *Chem. Phys.*, 2007, **333**, 236–245.
31 J. Olmsted and M. Strand, *J. Phys. Chem.*, 1983, **87**, 4790–4792.
32 P. Cadiot and W. Chodkiewicz, *Chemistry of acetylenes*, M. Dekker, 1969.
33 V. Enkelmann, in *Polydiacetylenes*, Springer, Berlin, Heidelberg, 1984, pp. 91–136.
34 G. Wegner, *Die Makromolekulare Chemie*, 1972, **154**, 35–48.
35 D. J. Ahn and J.-M. Kim, *Acc. Chem. Res.*, 2008, **41**, 805–816.
36 Y. Lifshitz, A. Upcher, O. Shusterman, B. Horovitz, A. Berman and Y. Golan, *Phys. Chem. Chem. Phys.*, 2009, **12**, 713–722.
37 A. A. Deckert, L. Fallon, L. Kiernan, C. Cashin, A. Perrone and T. Encalarde, *Langmuir*, 1994, **10**, 1948–1954.
38 S. Spagnoli, J.-L. Fave and M. Schott, *Macromol.*, 2011, **44**, 2613–2625.
39 R. Lécuiller, J. Berréhar, C. Lapersonne-Meyer, M. Schott and J.-D. Ganière, *Chem. Phys. Lett.*, 1999, **314**, 255–260.
40 R. Lécuiller, J. Berréhar, J. D. Ganière, C. Lapersonne-Meyer, P. Lavallard and M. Schott, *Phys. Rev. B*, DOI:10.1103/PhysRevB.66.125205.
41 Y.-H. Gong, F. Miomandre, R. Méallet-Renault, S. Badré, L. Galmiche, J. Tang, P. Audebert and G. Clavier, *Eur. J. Org. Chem.*, 2009, **35**, 6121–6128.
42 M. Cardona, R. V. Chamberlin and W. Marx, *Ann. Phys.*, 2007, **16**, 842–845.
43 M. Berberan-Santos, E. N. Bodunov and B. Valeur, *Ann. Phys.*, 2008, **17**, 460–461.
44 M. N. Berberan-Santos, E. N. Bodunov and B. Valeur, *Chem. Phys.*, 2005, **315**, 171–182.
45 M. Louis, C. Piñero García, A. Brosseau, C. Allain and R. Métivier, *J. Phys. Chem. Lett.*, 2019, **10**, 4758–4762.
46 L. Juhasz, R. D. Ortuso and K. Sugihara, *Nano Lett.*, 2021, **21**, 543–549.
47 G. M. Sheldrick, *University of Göttingen, Gôttingen, Germany*.
48 G. M. Sheldrick, *Acta Cryst A*, 2008, **64**, 112–122.
49 L. J. Farrugia, *J Appl Cryst*, 1999, **32**, 837–838.